Arabian Journal for Science and Engineering (2018) 43:6609–6625
https://doi.org/10.1007/s13369-018-3415-8

RESEARCH ARTICLE - PETROLEUM ENGINEERING

Mechanistic Modeling of Nanoparticles-Assisted Surfactant Flood

Seyyed Shahram Khalilinezhad[1] · Sina Mobaraki[2] · Mahdi Zakavi[2] · Milad Omidvar Sorkhabadi[3] · Goshtasp Cheraghian[4] · Khosro Jarrahian[5]

Received: 8 July 2017 / Accepted: 24 June 2018 / Published online: 7 July 2018

Abstract
High interfacial tension (IFT) between oil and water brings about high capillarity leading to high residual oil saturation. Surfactants are employed to reduce IFT or modify wettability and mobilize the trapped oil. This paper aims to investigate the interaction of sodium dodecyl sulfate as a surfactant and two types of silica nanoparticles in different particle sizes for the purpose of enhancing oil recovery. Accordingly, the effect of employed nanoparticles on the critical micelle concentration (CMC) of the surfactant was investigated by the use of electrical conductivity measurements. Phase behavior studies were also carried out to examine the solubilizing ability of the surfactant and nanoparticles assembly. Based on the analysis of solubilization curves, an ultra-low IFT chemical formulation for the target reservoir crude oil was identified and the stability of the optimum solutions was examined through visual observation, optical absorption, and zeta potential measurements. The oil recovery experiments were performed in a quarter five-spot transparent pore network model saturated with crude oil to observe the displacement behavior of the injectant and its influence on oil recovery. Phase behavior tests indicated that the silica nanoparticles smaller in size are more effective in terms of IFT reduction since they can achieve ultra-low IFT level, and the conductivity measurements showed they relatively reduce the CMC of the surfactant. The results of stability tests demonstrated the optimum solutions are stable for more than 1 week. The micromodel experiments displayed that oil recovery increased by 4% during nanoparticles-assisted surfactant flood in comparison with surfactant flood.

Keywords Surfactant flood · Oil recovery · Nanoparticles · Solubilization

Nomenclature

2D	2-Dimensional
ASP	Alkaline–surfactant–polymer flood
CSEL	Lower effective salinity window
CSEU	Upper effective salinity window
TEM	Transmission electron microscope
UTCHEM	The University of Texas at Austin Chemical Flood Simulator

List of symbols

HBNC70	UTCHEM input parameter for surfactant model (intercept of maximum height of binodal curve at zero salinity [44])
HBNC71	UTCHEM input parameter for surfactant model (intercept of maximum height of binodal curve at optimal salinity [44])
HBNC72	UTCHEM input parameter for surfactant model (intercept of maximum height of binodal curve at twice optimal salinity [44])
CSEL7	UTCHEM input parameter for surfactant model (lower critical salinity window [44])
CSEU7	UTCHEM input parameter for surfactant model (upper critical salinity window [44])

✉ Seyyed Shahram Khalilinezhad
sh.khalilinezhad@eqbal.ac.ir

[1] Department of Petroleum Engineering, Eqbal Lahoori Institute of Higher Education, Mashhad, Iran

[2] Young Researchers and Elites Club, Science and Research Branch, Islamic Azad University, Tehran, Iran

[3] Department of Petroleum Engineering, Quchan Branch, Islamic Azad University, Quchan, Iran

[4] Young Researchers and Elites Club, Omidiyeh Branch, Islamic Azad University, Omidiyeh, Iran

[5] Institute of Petroleum Engineering, Heriot Watt University, EH14 2SQ Edinburg, UK

1 Introduction

The discovery of new huge stocks of crude oil is becoming less and less frequent, and advanced technologies are needed

to increase the oil production due to the rise in the world's oil demand. Chemical enhanced oil recovery (CEOR) has increasingly come into focus as one of the improved oil recovery processes that have the potential to produce oil with relatively low cost from mature reservoirs [1]. It involves the use of chemicals such as surfactant, co-solvents, polymer, and alkaline agents to mobilize residual oil trapped in pores and pore throats. Among different CEOR methods, surfactant flooding is a promising enhanced oil recovery (EOR) technique bringing about the oil/aqueous IFT to drop, thus allowing emulsification and displacement of the unswept oil in the reservoir. In fact, surfactants reduce the IFT between oil and water from the waterflood range of 25–30 mN/m, leading to an increase in the capillary number and bringing about a vast reduction in oil saturation [2]. Particularly, when surfactant, water, and oil are mixed together, they form a thermodynamically stable phase called microemulsion characterized by ultra-low IFT and the ability to solubilize both aqueous and oil compounds. In addition, in order for the solubilization mechanism to be more effective, the surfactant concentration should be higher than critical micelle concentration (CMC) during the flow of the mixture through porous media [3]. As the effect of microemulsions on oil recovery has attracted extensive attention, there is rich literature on the improved oil recovery through solubilization mechanism [4,5]. Winsor [6] classified the microemulsions into three different types, Type I, Type II, and Type III. The type of microemulsion depends on salinity, ionic species, surfactant concentration, and other key factors. The details of different microemulsion types, their properties, and classifications are completely documented elsewhere [2]. It is generally believed that, except for Yassin et al. [7] who stated that Type III of microemulsion is not necessarily the optimum phase corresponding to the highest oil recovery, Type III of microemulsion is more suitable for CEOR because of the corresponding low and equal IFT between this phase and the excess phases of oil and water [8–10]. It is worthwhile to note that one of the most widely used correlations [11] to calculate the relations between IFTs and solubilized oil and brine volumes with high level of accuracy compared with experimental data has been presented by Huh [12]. Due to the well-established relationship between the microemulsion phase behavior and IFT, it is common in the industry to screen surfactants and their formulations for low IFT through oil–water phase behavior tests. Accordingly, great deals of the research efforts have focused on the importance of phase behavior studies in chemical flooding [13,14]. Healy et al. [15] showed that the phase behavior of surfactant/brine/oil system is a crucial factor in interpreting the performance of oil recovery during surfactant flooding. Moreover, they found that low IFT and high solubilization of both oil and water in the microemulsion phase occur in or near the salinity ranges giving three phases. Hirasaki et al. [16] reported the importance of salinity gradient concept in surfactant flooding by the use of comprehensive phase behavior studies. They stated that when the salinity gradient is used, the surfactant retention is minimal and the salinity of chemical slug is at optimum for enhancing oil recovery. Levitt et al. [17] conducted the experimental phase behavior studies for screening the high-performance and low-cost surfactants. Their results demonstrated that phase behavior screening helps to quickly identify favorable surfactant formulations. In addition, branched alcohol propoxy sulfates, internal olefin sulfonates, and branched alpha olefin sulfonates have been identified as good EOR surfactants.

As the surfactant's performance is a function of reservoir condition, some studies have discussed the role of effective additives in improvement in surfactant properties for CEOR applications. Dwarakanath et al. [18] carried out the oil recovery experiments and also phase behavior studies for the evaluation of the effect of co-solvents on the improvement in both light oil recovery and phase behavior of microemulsions. They employed a chemical compositional reservoir simulator to match both phase behavior and oil recovery experiments. They stated that by adding the appropriate co-solvent and the correct amount of electrolyte in the chase solutions, more than 90% of IOIP could be recovered and Winsor Type III condition for extended durations even with a small surfactant slug could be maintained. Awang et al. [19] suggested that the branched alcohols can be used as an effective additives to improve the performance of anionic surfactant in terms of IFT reduction. They showed that adding even a small amount of the branched alcohols to the injectant can reduce the IFT of oil/surfactant solution dramatically for both low and high salinity conditions.

Researchers have also reported recent advances in the results of the improved properties of chemical agents by the use of different nanoparticles [20,21]. Zargartalebi et al. [22] and Zargartalebi et al. [23] investigated the capability of silica nanoparticles for the enhancement of surfactant flooding performance. They conducted different adsorption and IFT measurements and observed that dispersed silica nanoparticles in surfactant (DSNS) solution can reduce the amount of surfactant adsorption and also improve the IFT behavior of surfactant/crude oil system. Vatanparast et al. [24] investigated the effect of combined interfacial and bulk properties of silica nanoparticles and a cationic surfactant mixture in water/oil systems when the surfactant/nanoparticles ratio is low. They presumed that hydrophilic silica nanoparticles are not surface active alone and have no significant effect on water/heptane IFT. However, in the presence of a cationic surfactant, nanoparticles become surface active complexes by adsorbing surfactant molecules and strongly affect the interfacial properties. They experimentally showed that the system containing both surfactant and nanoparticles has lower

equilibrium IFT and the IFT decreases with the increase in nanoparticles concentration. Biswal et al. [25] explored the effect of negatively charged silica nanoparticles on the IFT of the n-hexane–water system at various concentrations of different surfactants. They experimentally demonstrated that the employed nano-sized additives have different effects depending on the type of surfactant. The results showed that the silica nanoparticles can reduce the IFT of anionic surfactant/oil dramatically while the reverse trend was observed for the nonionic surfactant. Esmaeilizadeh et al. [26] studied IFT behavior of systems containing both surfactant and zirconium dioxide (ZrO_2) nanoparticles. They displayed that at water–air interface, inclusion of the nanoparticles dramatically improved the surface activity of anionic surfactant molecules and had negligible effect on the surface tension of both cationic and nonionic surfactants. Ahmadi et al. [27] examined the impacts of hydrophobic silica nanoparticles on the ultimate oil recovery of carbonate cores. They showed that the injection of this type of nanoparticles can improve oil recovery considerably and this improvement was directly related to the unique IFT behavior of nanofluid/oil system. They also reported that there was an optimum concentration of about 2500 ppm for the application of nanoparticles in EOR processes. AlamiNia et al. [28] performed a study concerning the role of hydrophilic silica nanoparticles in the performance of both surfactant and polymer solutions. They experimentally proved that the addition of silica nanoparticles to the surfactant solution has a significant impact on both the stability and IFT behavior of the surfactant solution. By the use of solubilization curves, they stated that the smaller the size of nanoparticles are, the more effective the performance of anionic surfactant in reducing IFT of oil/water system will be. Ahmadi et al. [29] evaluated the effect of silica nanoparticles on the CMC of a natural surfactant by the use of conductivity approach. They showed that CMC of the employed surfactant decreased while the concentration of nanoparticles increased.

Cheraghian et al. [30] studied the effect of dispersed clay nanoparticles in surfactant solution on heavy oil recovery. By the use of an extensive experimental research, they found that dispersed clay nanoparticles can improve both oil recovery and adsorption behavior of surfactant solution, especially near to CMC condition during surfactant flooding. Ahmadi et al. [31] presented the experimental observations on the effect of two different types of silica nanoparticles on adsorption behavior of SDS. Their conductivity measurements revealed both nanoparticles having a strong ability to decrease the amount of surfactant adsorption onto the sandstone rocks, but the hydrophobic silica nanoparticles are more effective than hydrophilic silica nanoparticles.

Cheraghian et al. [32] conducted an experimental study to monitor the interaction of SDS surfactant and fumed silica nanoparticles as suitable agents for oil displacing in EOR by the use of glass micromodels. They concluded that the addition of nanoparticles enables a further 13% enhancement in oil recovery as well as delaying the breakthrough time. They also suggested the wettability of porous medium surface can be dramatically improved by the use of surfactant and nanoparticles assembly.

In the present study, for a better understanding of the interaction of SDS as a surfactant and two types of silica nanoparticles in different particle sizes, conductivity measurements and phase behavior tests are performed and the ability of the solution containing both surfactant and nanoparticles is investigated in terms of oil emulsification and IFT reduction. Afterward, the stability of the optimum formulations is evaluated by the use of several methods such as visual observations, optical absorption, and zeta potential measurements. Then, the optimum solution is injected into the five-spot glass micromodel to observe the quantitative and qualitative efficiency of the newly formulated system for improving oil recovery. Finally, based on the phase behavior data, the surfactant module of a compositional chemical flood simulator (UTCHEM) is tuned and the oil recovery results are also modeled by the use of UTCHEM simulator which has the ability to simulate the flow of microemulsion phase through porous media.

2 Methodology

2.1 Materials and Procedures

The surfactant used in this study was an anionic surfactant named sodium dodecyl sulfate (SDS) with the purity above 99% obtained from Merck Company. The main properties of the surfactant are given in Table 1. Two types of hydrophilic silica nanoparticles with different particle sizes were used in this work. The first one with smaller particle size was AEROSIL 300 provided by Evonik Company, and the other was silicon dioxide nanopowder obtained from US Nanoresearch, Inc. Based on the manufacturer's reports, they are well-characterized hydrophilic fumed silica which is prepared by hydrolysis of silica tetrachloride in which silanol group (Si–OH) is generated on the silica surface. Moreover, regarding the preparation procedure reported by manufacturer, both nanoparticles implemented throughout this research are made from SiO_2 and some additives such as Al_2O_3, Fe_2O_3, and TiO_2. The properties of the nanoparticles are summarized in Table 2. Deionized (DI) water was used as the aqueous phase. The non-reactive (with low acid number) and relatively light crude oil from one of the Iranian oil fields, located in southwest of Iran, was used as the oil phase. The crude oil has the API of 27 and viscosity of 29 mPa s at standard condition. Sodium chloride (NaCl) with

Table 1 Properties of anionic surfactant used in this study

Solubility (g/l)	Density (g/cm^3)	Flash point (°C)	pH Value	Bulk density (kg/m^3)
150	1.1	> 150	6–9	490–560

Table 2 Properties of nanoparticles used in this study

Type	SiO_2 (wt%)	Particle size (nm)	Specific area (m^2/g)	Tamped density (g/l)
AEROSIL 380 (hydrophilic)	> 99.5	7	380	50
Silicon dioxide nanopowder (hydrophilic)	99.5	20–30	160–600	0.002

99% purity was also provided by Merck Company and used for the preparation of brine.

X-ray diffraction (XRD) is a common technique for the study of crystal structures and atomic spacing. As a result, by using XRD patterns, the crystalline structure of nanomaterials can be also described. In this research, XRD patterns of the two types of silica nanoparticles were recorded by diffractometer (Philips Analytical X-ray, CuKα, $\lambda = 1.54184$, Step size $= 0.02$, and scan step time $= 0.4$ s). In addition, for characterizing the two types of hydrophilic silica nanoparticles utilized in this study, transmission electron microscopy (TEM) was used to specify the particle size with a Philips CM120.

Figure 1 shows the XRD patterns of the two different employed silica nanoparticles. Based on the presented patterns for both nanoparticles, the curve of scattered intensity versus 2θ showed nothing more than one broad maxima which indicated the characteristics of amorphous nature of silica particles and as a result proved the high purity of the silica nanoparticles [33]. We also used TEM analysis to estimate an average value for the particle size of nanoparticles. This analysis showed that their average size is of order of few nanometers.

The method used for nanoparticle dispersion is of great significance since the solution properties are highly dependent on this method. Ultrasonication method using ultrasonic waves with the specific power and frequency is one of the best ways for characterization, synthesize and dispersion of nanomaterials such as silica nanoparticles [34]. Accordingly, silica nanoparticles were dispersed in DI water by means of ultrasonic apparatus (Sonic, VCX750). In addition, accurate amounts of surfactant powder were added slowly to the silica nanoparticles solution while stirring on a magnetic stirrer (IKA). The crude oil was centrifuged by the use of HERMLE centrifuge (Z36HK). To analyze optical absorbance of nanoparticle-augmented surfactant solutions with different salinities, the ultraviolet–visible spectrometer (UV–visible, CT-5700) was used. This technique is a reliable method to investigate the nanosuspension stability [35]. A nanosizer-ZS (Nano ZS, Malvern Instruments, UK) equipped with helium neon laser (633 nm) was used to obtain the zeta potential of particles in each solution. Zeta potential data are required to decide the charge nature of the particle surfaces, surfactant–molecular interactions, and the estimation of solution stability.

The estimation of the CMC of the surfactant in the aqueous solution is strongly dependent on different intrinsic characteristics of surface active agents, such as surface tension, thermal conductivity, and electrical conductivity [36]. Based on the high electrical conductance of the introduced surfactant in aqueous solutions, the electrical conductivity measurement was selected as a robust method to determine the micellization behavior of the introduced surfactant with and without nanoparticles in aqueous solutions. Accordingly, conductivity measurements were taken by a conductivity detector (Seven easy, Mettler Toledo, Switzerland).

IFT of crude oil was measured against DI water by means of Kruss tensiometer (K100). This tensiometer can determine IFT of oil against water by the use of ring method in the range of 1–1000 mN/m [37]. Phase behavior or pipette tests were also conducted in small tubes called pipettes to find optimum chemical formulation. To perform oil recovery experiments, one-quarter five-spot glass micromodel was designed similar to the Ghahremani et al. [38]. The schematic representation of the micromodel setup is shown in Fig. 2. The 2D micromodel was fabricated based on a method using laser technology. Procedure details of micromodel construction can be found elsewhere [39]. The pattern of micromodel was prepared by a thin section of a heterogeneous sandstone rock from one of the Iranian oil reservoirs. Physical properties of the micromodel are also given in Table 3.

To prepare nanoparticle-augmented surfactant solutions (nanoparticle size of 7 nm), 0.25 g silica nanoparticles were added to 100 cm^3 of DI water, meaning that the concentration of silica nanoparticles was equal to 2500 ppm, stirred slowly for 1 h. This concentration was suggested as an optimum concentration of hydrophilic silica nanoparticles by many researchers for CEOR applications [27,28,40]. Then, 0.5 g solid SDS was added to 50 cm^3 of the prepared aqueous

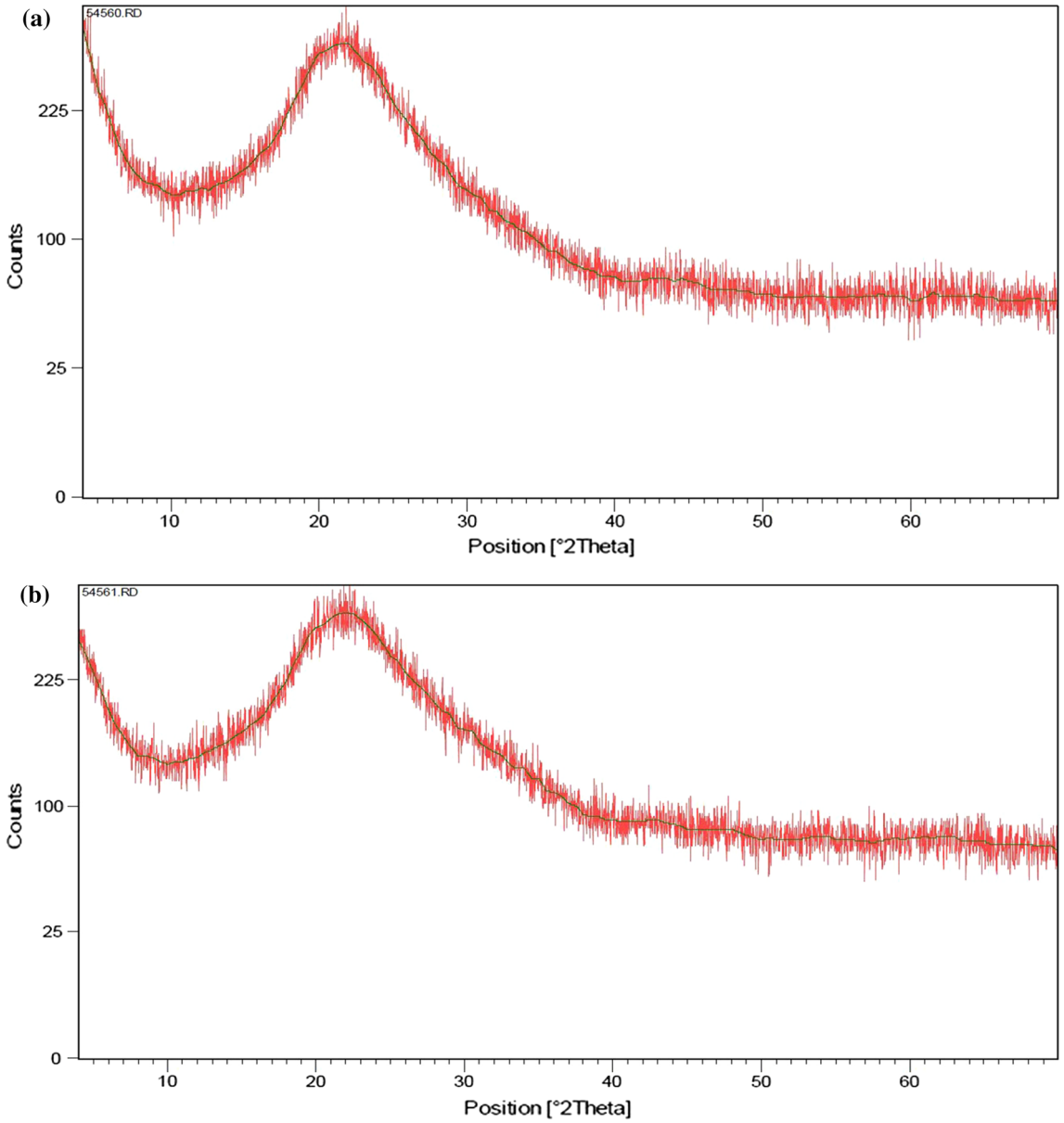

Fig. 1 XRD pattern of two types of silica nanoparticles used in this work, **a** silica nanoparticles with the particle size of 7 nm and **b** silica nanoparticles with the particle size of relatively 25 nm

nanosilica solution, which means that the SDS concentration was equal to 10,000 ppm, and the solution was stirred again for 1 h. The aqueous nanoparticles-augmented surfactant solution was sonicated by the means of ultrasonic apparatus for 45 min. Based on the reported compositions of the reservoir fluids, NaCl is the main component of the reservoir brine (Table 4). Accordingly, to prepare chemical solutions with different salinities, a wide range of salt concentrations (NaCl) were used (5000, 10,000, 15,000, 20,000, 30,000, 40,000, 50,000, 60,000, 70,000 ppm). Finally, a desirable amount of salt was dissolved in the prepared solution and the resultant solution was stirred for 60 min by the use of magnetic stirrer. The similar procedure was performed for the case of silica nanoparticles with the particle size of 25 nm. Moreover, to prepare surfactant solutions without silica nanoparticles, 1 g solid SDS was added to 100 cm^3 of DI water, meaning that the concentration of SDS was equal to 10,000 ppm, and stirred slowly for 1 h. Then, a desirable amount of salt (similar to nanoparticle-augmented surfactant solutions) was dissolved in the prepared solution, and the resultant solution was stirred for 60 min by the use of magnetic stirrer.

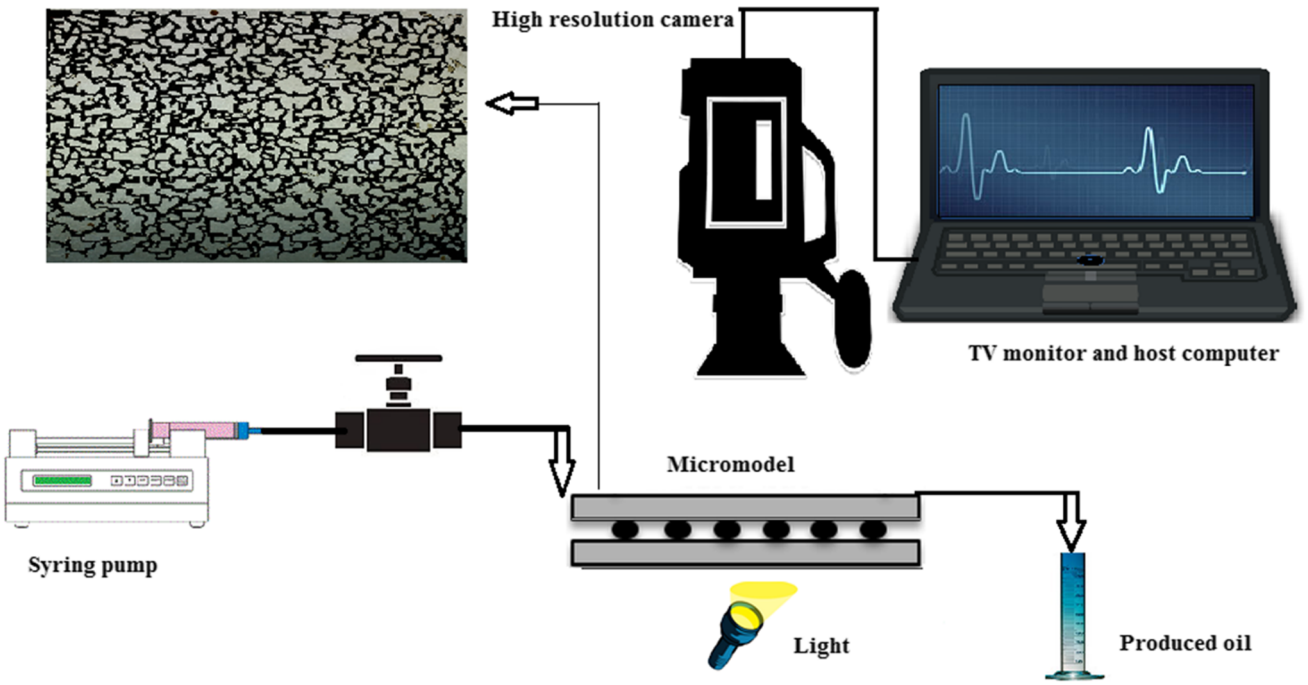

Fig. 2 Schematic of glass micromodel setup

Table 3 Physical properties of glass micromodel

Length (cm)	Width (cm)	Thickness (cm)	Porosity	Absolute permeability (D)
5.98	5.98	0.0141	0.46	0.5

Table 4 Composition of the reservoir brine

Composition	Weight (%)
NaCl	2.45
Na_2SO_3	0.005
$CaCl_2$	0.01
$MgCl_2 \cdot 6H_2O$	0.02
Na_2HCO_3	0.01

2.2 Methods

2.2.1 Emulsification Ability of DSNS Solution

The phase behavior of surfactant–oil system is the important step in the laboratory to screen the proper surfactants for CEOR. Generally, aqueous stability tests are performed prior to the salinity scan tests in order to find the salinity at which the solubility limit reached. This is important since the surfactant solution needs to be stable up to at least the optimum salinity.

In this study to accomplish an aqueous stability test, based on the prepared 18 nanoparticle-augmented surfactant solutions, 5 ml of each sample was pipetted into a graduated 10-ml vial. Then, the crude oil was centrifuged first for 45 min at 2000 rpm to separate a small amount of brown-colored phase which was suspected to be emulsified oil, and 5 ml of crude oil was added to the vial (water–oil ratio or WOR equal to unity). It should be mentioned that temperature (equal to 25°C), SDS concentration, and silica nanoparticles concentration were fixed, whereas the concentration for NaCl varied in different test tubes because the effect of salinity on the phase behavior of surfactants is one of the important variables of the surfactant flooding, and as a result, salinity is the main variable in this research. Pressure was also assumed to be a minor effect, and it is generally atmospheric. After that, the test tubes were gently agitated to facilitate mixing of fluids. Next, they were left in a transparent bottle away from degrading factors such as light and heat. The level of fluid interfaces was recorded periodically, at intervals ranging from 1 to 8 days for observing equilibrium. Then, according to the equilibrium level of fluids, the solubilization curves were determined and drawn. Finally, the type of microemulsion changes as the salinity increases. It should be noted that the salinity at equal volumes of oil and water solubilized in the microemulsion is defined as the optimal salinity. The optimal salinity is approximately at the midpoint between upper and lower effective salinities [2]. The procedures used to measure the microemulsion phase behavior, determine solubility

curves parameters, and criteria to screen chemical formulations are completely illustrated elsewhere [41,42].

In this work, Winsor nomenclature was used to represent surfactant phase behavior. Accordingly, surfactant/microemulsion phase behavior is described as Winsor type I, type II, and type III. A transition in phase behavior can be the result of a change in variables such as salinity, temperature, equivalent alkane carbon number (EACN) of the oil, or surfactant structure. Based on the Huh (1979) equation [12] examined by many researchers for numerous combinations of surfactant and crude oil over a wide range of temperature, salinity, and concentration [2], IFT is inversely proportional to the square of the solubilization ratio:

$$\gamma = \frac{C}{\sigma^2}, \tag{1}$$

where C is approximately 0.3 and the solubilization ratio (σ) is defined as the volume of oil or water solubilized divided by the volume of surfactant on a 100% active basis. Achieving ultra-low IFT on the order of 10^{-3} mN/m is necessary to mobilize the residual oil saturation in reservoir rocks. Solubilization ratio is much more easily and accurately measured over time than IFT, and therefore, it is a useful method for measuring IFT directly [2].

Moreover, the conductivity measurements were also taken to measure the CMC of the optimum solutions and evaluate the effect of adding hydrophilic silica nanoparticles on the minimum surfactant concentration required for oil emulsification compared with the surfactant solution without dispersed silica nanoparticles. It should be noticed that in this section the effect of silica nanoparticles on CMC of surfactant was investigated in the absence of salt due to the presence of divalent and monovalent ions having a considerable effect on the electrical conductivity of the solutions [29].

2.2.2 Stability of DSNS Solution

After evaluating the prepared solutions by analyzing the solubilization curves, the stability of the nanoparticle-augmented surfactant solutions was investigated by the use of ultraviolet–visible spectrophotometer and zeta potential experiments. Consequently, the optical absorbance of the solutions was measured in different periods of time (1, 6 h, 2, and 8 days). It should be mentioned that the absorbance–time relationship provides a method to study the aggregation of silica dispersions [35]. In addition, zeta potential tests were also performed, just after the preparation of the solutions, to examine the effect of the interaction of components on the solution stability.

2.2.3 Oil Recovery Experiments

The oil recovery experiments were performed by a quarter five-spot glass micromodel since the microscopic efficiency as well as macroscopic behavior of the chemical flooding was required to be studied. The micromodels are transparent artificial models of porous media that can be utilized to simulate the fluid flow processes at the pore scale. The main objective of micromodel utilization is to observe the fluid flow through porous media. As a result, a heterogeneous quarter five-spot glass micromodel composed of a micromodel holder placed on a platform, a high-resolution camera, and a precise low-rate syringe pump used to control the flow rate of fluids throughout the micromodel was utilized. Fluid saturations were observed by taking high-quality pictures and then analyzed by using image processing software in combination with a developed computer code.

Before each experiment, the micromodel was cleaned with toluene and deionized water. In this study, the procedure to restrain the initial water-wet state of the micromodel is the same as the procedure used by Emami Meybodi et al. [43]: (1) rinse the micromodel with toluene to eliminate any residual oil and then use a vacuum pump to remove any remaining liquids from the micromodel, (2) rinse the micromodel with acetone and remove any remaining fluids using the vacuum pump, (3) rinse the micromodel with distilled water and remove any remaining water, (4) soak the micromodel in hydrochloric acid solution (20% acid, 80% water by volume) for several hours, (5) remove any remaining acid from the micromodel and rinse it with distilled water and again remove any remaining water, (6) rinse the micromodel with acetone and remove any remaining acetone, and (7) dry the micromodel using an oven set at a temperature of 100°C for 1 h. It should be mentioned that the porosity of the micromodel was estimated to be $0.46 \pm 0.05\%$ using a combination of image analysis and the average etched depth. The image analysis was used to estimate the areal porosity of the model when it was filled with water. The absolute permeability of the model was calculated equal to 500 md $\pm$ 0.05% by using Darcy's law and introducing different flow rates and recording the related pressure drop. By plotting flow rate versus pressure drop across the pattern and fitting best line passed through the origin for this set of data, slope of the line will yield the value of absolute permeability by having viscosity of the flowing fluid (water) and length and cross-sectional area of micromodel.

Next, micromodel was saturated with water and then saturated with the reservoir crude oil to create the condition of connate water saturation. The first displacement test was water flooding into the micromodel. Using image analysis, recovery efficiency was measured in terms of the injection time. During the oil recovery experiments, microscopic pictures were continuously taken from the micromodel to

visualize fluid distribution in pores. At the end of the first experiment, the micromodel was cleaned up by toluene and ethanol and then dried in an oven set at temperature of 120°C for 2 h. Before, the second test (surfactant flood), the micromodel was saturated with heavy oil again and all the mentioned steps for the water flood carried out. It should be mentioned that the same procedure was used for the DSNS flood experiments. It should be considered that all experiments were carried out at room temperature and pressure and on a horizontal surface. According to the saturation process, the connate water saturation was less than 4%. In addition, the injection rate was fixed at 0.0015 cc/min. This flow rate relatively simulates fluid flow velocity in the oil reservoirs.

2.3 Numerical Model

UTCHEM [44] as a three-dimensional, multiphase, multicomponent chemical flooding simulator is used in this paper. Based on the chemical EOR benchmark study published by Goudarzi et al. [45], UTCHEM is the unique simulator which has the capability of modeling of microemulsions phase behavior. Here, we briefly describe the surfactant module of UTCHEM.

2.3.1 Microemulsion Viscosity

Viscosity of microemulsion phase is one of the most important parameters influencing the performance of surfactant-based EOR techniques. Microemulsion viscosity is strongly dependent on the composition of its components. UTCHEM can model microemulsion viscosity as a function of water, oil, and surfactant concentrations in the microemulsion phase shown as follows [44]:

$$\mu_{\mathrm{ME}} = C_{13}\mu_w \mathrm{e}^{[\alpha_1(C_{13}+C_{23})]} + C_{23}\mu_o \mathrm{e}^{[\alpha_2(C_{13}+C_{33})]} + C_{33}\alpha_3 \mathrm{e}^{[\alpha_4(C_{13}+C_{33})]} \quad (2)$$

where C_{13}, C_{23}, and C_{33} are water, oil, and surfactant concentration in the microemulsion phase; α_1, α_2, α_3, α_4, and α_5 are input parameters, and they are adjusted until a satisfactory fit of the measured viscosity and the model is obtained. When polymer is added to the surfactant solution, water viscosity μ_w is replaced with polymer solution viscosity. Due to the lack of microemulsion viscosity laboratory measurements, Fig. 3 represents the relationship of microemulsion viscosity as a function of oil solubilization ratio, and we used these common values [46] for our simulations.

2.3.2 Interfacial Tension

IFT reduction is a function of surfactant type and surfactant concentration among other key parameters [47]. Healy and Reed [48] and also Huh [12] correlations are available options for calculating IFT during surfactant flooding. Huh correlation, which was used in this study, is as follows:

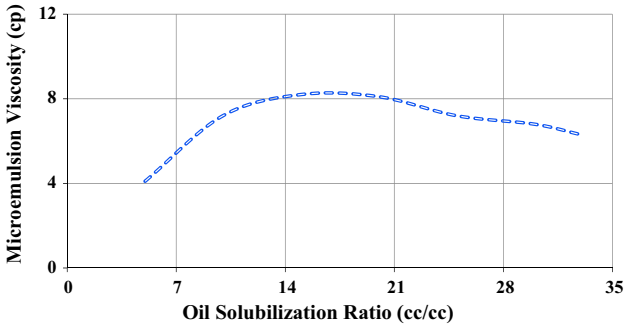

Fig. 3 Assumed (based on [46]) microemulsion viscosity as a function of oil solubilization ratio

$$\sigma_{13} = \sigma_{\mathrm{ow}} \mathrm{e}^{[-aR_{l3}]} + \frac{CF_l}{R_{l3}^2}\left(1 - \mathrm{e}^{-aR_{l3}^3}\right), \quad (3)$$

where σ_{ow} is oil/water IFT and F_l is the correction factor which is used to ensure the IFT approaches oil/water IFT in the absence of surfactant, and is equal to about 10. C is a constant which is equal to 0.3 and R is the solubilization ratio. It should be noticed that subscript l refers to the oleic phase.

2.3.3 Phase Behavior

Phase behavior of surfactants is affected by reservoir condition, and many factors control the performance of surfactant flooding. The phase behavior model in UTCHEM is based on Hand's rule [49] and uses the ternary diagram to represent different microemulsion phases and tie lines [44]. The equations derived from Hand's model for phase behavior calculations are solved using the height of binodal curve as input parameters. The input parameters in UTCHEM which represent the height of binodal curve are HBNC70, HBNC71, HBNC72, which are the height of binodal curve at zero, optimum, and twice optimum salinity conditions, respectively. The values of these parameters are obtained by matching the laboratory measured phase behavior data through a developed a spreadsheet [46,50] or conventional batch simulations [51,52].

2.3.4 Construction of Numerical Model

The UTCHEM simulator was used to history match oil recovery data for both water flooding and chemical flooding. The numerical model uses 40 grid blocks for each x and y directions with one grid block in z direction. Based on the physical properties of micromodel summarized in Table 3, each grid block in numerical model has the 0.149 cm length, 0.149 cm

width, and 0.0140 cm thickness. The phase behavior data of the optimum solution were imported to the simulator to simulate the DSNS flood. It should be mentioned that the surfactant adsorption module of UTCHEM was tuned and the required adsorption data for simulation of surfactant flood were based on the adsorption behavior of DSNS solution reported by Zargartalebi et al. [23].

Clearly, the oil recovery is related particularly to the properties of relative permeability curves which are strongly a function of IFT. UTCHEM uses Corey-type relative permeability for aqueous, oleic, and microemulsion phases [44]. In this study, residual saturations, endpoints, and exponents of relative permeability curves for each phase were modified based on the history match of oil recovery experimental results. Based on the ability of DSNS solutions in reducing IFT, relative permeability curves were defined as a function of capillary number (one set of relative permeability curves for each high capillary number and low capillary number conditions) and both of the curves were tuned for DSNS flood. As a result, a few relative permeability exponents and endpoints for both oil and water phases were tested in an acceptable range of apparatus.

3 Results and Discussion

3.1 IFT Measurements

Before conducting phase behavior experiments, the IFT between crude oil and DI water was measured at ambient temperature using Kruss tensiometer. Figure 4 shows the IFT as a function of elapsed time. This figure shows that IFT of crude/DI water is relatively equal to 10 mN/m and it is unfavorable for oil displacement processes. It is believed that the IFT should be reduced to the order of 10^{-2} or 10^{-3} mN/m for flowing of oil droplets through pore throats more easily [2].

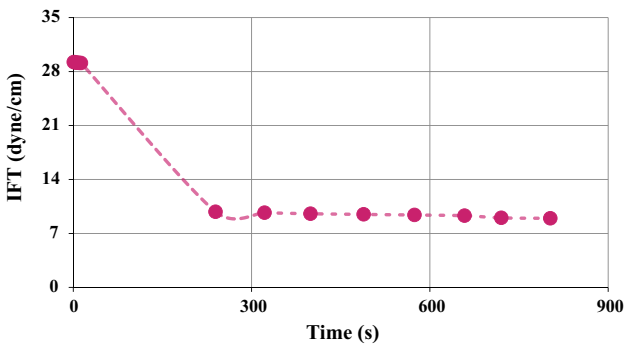

Fig. 4 IFT between crude oil and DI water as a function of elapsed time

3.2 Phase Behavior Experiments

Figure 5a, b displays the salinity scan tests for DSNS solutions. As the pictures show, some precipitation appears and the solution looks extremely hazy only for salinity equal to 70,000 ppm after 8 days of the preparation process. Based on the equilibrated phase volumes, for both DSNS solutions, the solubilization curves were also determined and the emulsification ability of both solutions was investigated. To determine input parameters for phase behavior model of UTCHEM simulator, we used the developed spreadsheet. As a result, the spreadsheet model was tuned by the use of experimental data and the results for both DSNS solutions are depicted in Fig. 6. In addition, the tuned parameters of phase behavior model for both DSNS solutions are given in Table 5.

Based on the results depicted in Fig. 6a, the solubilization ratio at the optimal salinity of about 22,000 ppm total dissolved solids (TDS) was about 12.5 for DSNS solution with the particle size of 7 nm. The IFT at the optimal salinity was estimated to be approximately 0.0018 mN/m using the solubilization ratio of 12.5 in the Huh's equation [12]. Moreover, aqueous surfactant solution was clear and stable up to 50,000 ppm for at least 8 days. Figure 6b shows the solubilization ratios of oil and water at different salinities after 8 days of equilibrium for DSNS solution with the particle size of 25 nm. As the results show, the solubilization ratio at the optimal salinity of about 38,000 ppm TDS was about 10.5 for this solution. The IFT at the optimal salinity was estimated to be approximately 0.0027 mN/m using the solubilization ratio of 10.5 in the Huh's equation [12]. Similar to the previous solution, aqueous surfactant solution was clear and stable up to 50,000 ppm for at least 8 days. These results show that both types of dispersed silica nanoparticles can improve the performance of SDS solution in terms of IFT reduction and oil emulsification. The proposed mechanism for the behavior of surfactant and silica nanoparticles assembly on IFT is that the repulsive electrostatic forces between the particles and the SDS promotes the surfactant diffusion toward the interface [22]. Another explanation is that particles covered by a large amount of surfactant can act as a carrier of SDS toward the interface. The reduction in IFT could be due to the effect of surfactant released from the particles [53] but could also be due to the effect of surfactant-coated particles on the surface tension [54]. In addition, based on the Huh [12] equation, our experimental results showed that silica nanoparticles smaller in size are more effective in terms of IFT reduction as they can achieve ultra-low IFT level (0.0018 mN/m).

3.3 Conductivity Measurements

As mentioned earlier, the conductivity measurement is one of the best ways for CMC determination. In fact, a turning point in the plot of electrical conductivity versus surfactant

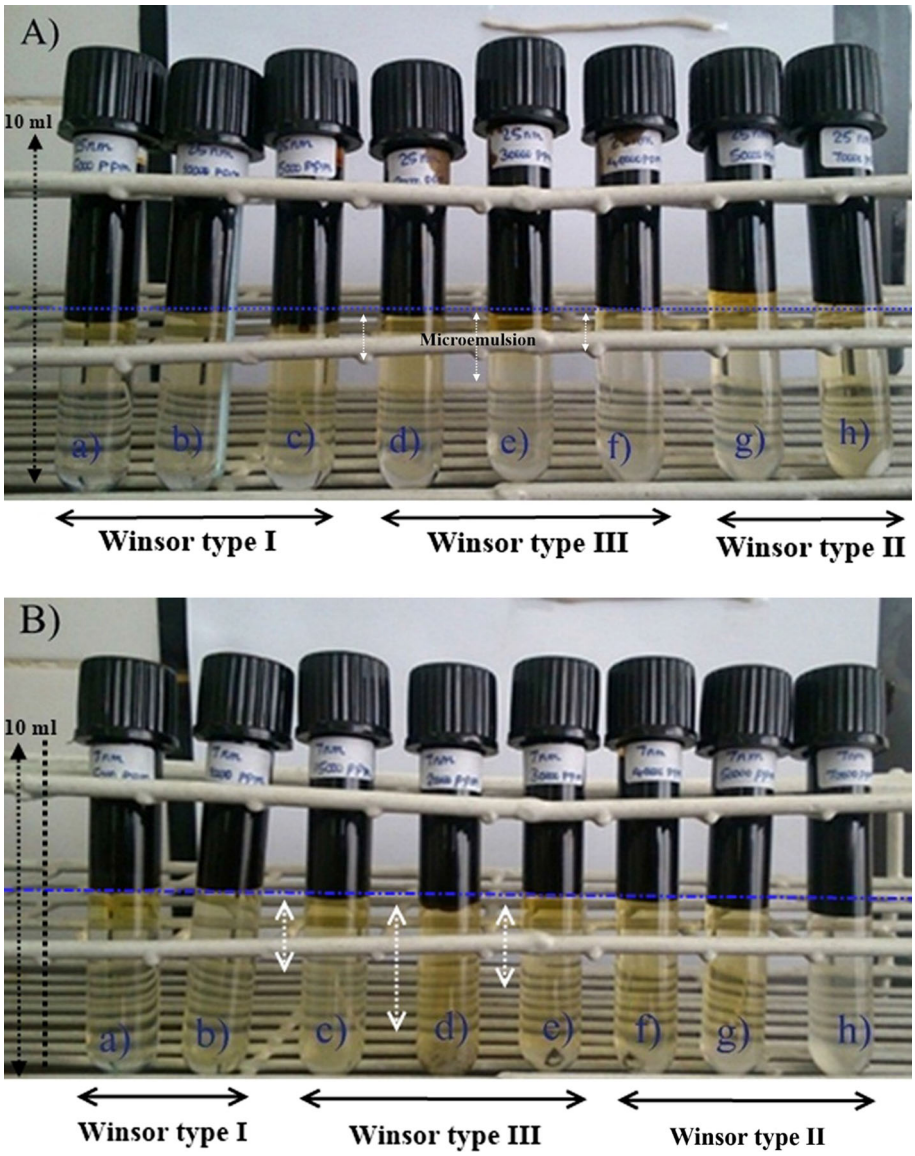

Fig. 5 Salinity scan tests for DSNS solutions (after 8 days of preparation), **a** DSNS of 25 nm, **b** DSNS of 7 nm (a: 5000 ppm NaCl, b: 15,000 ppm NaCl, c: 20,000 ppm NaCl, d: 30,000 ppm NaCl, e: 40,000 ppm NaCl, f: 50,000 ppm NaCl, g: 70,000 ppm NaCl)

concentration represents CMC of the surfactant solution. In this section, the probable changes in CMC of the surfactant with the existence of hydrophilic silica nanoparticles are investigated. Accordingly, nanoparticle-augmented surfactant solutions with different surfactant concentrations were prepared similar to the reported procedure in Sect. 2.1. Table 6 shows that CMC of the SDS solution without silica nanoparticles is about 2450 ppm and this result is in complete agreement with the related literature [36]. Table 6 also displays CMC of the DSNS solutions with silica nanoparticles of 7 and 25 nm, respectively. As the results show, CMC of surfactant is determined about 2100 ppm for DSNS solution with the particle size of 7 nm. In addition, CMC of surfactant is determined about 1850 ppm for DSNS solution with the particle size of 25 nm. As a result, it seems that the hydrophilic silica nanoparticles influenced the surfactant micellization properties, particularly its CMC. As can be seen, the coexistence of SDS and hydrophilic silica nanoparticles in a solution led to a CMC value lower than the one for the SDS solution without silica nanoparticles. These figures show that the presence of the employed silica nanoparticles resulted in surfactant molecules aggregating into micelles at lower concentrations. This phenomenon is more significant for silica nanoparticles with larger particle sizes. The observed trends may be related to the surfactant–nanoparticle interactions. Ignoring the small amount of surfactant adsorption on the surface of nanoparticles, the similar negative electrical charge on the surfactant head groups and the surface of nanoparticles results in an electrostatic repulsion between surfactant molecules toward each other, thereby improving the micel-

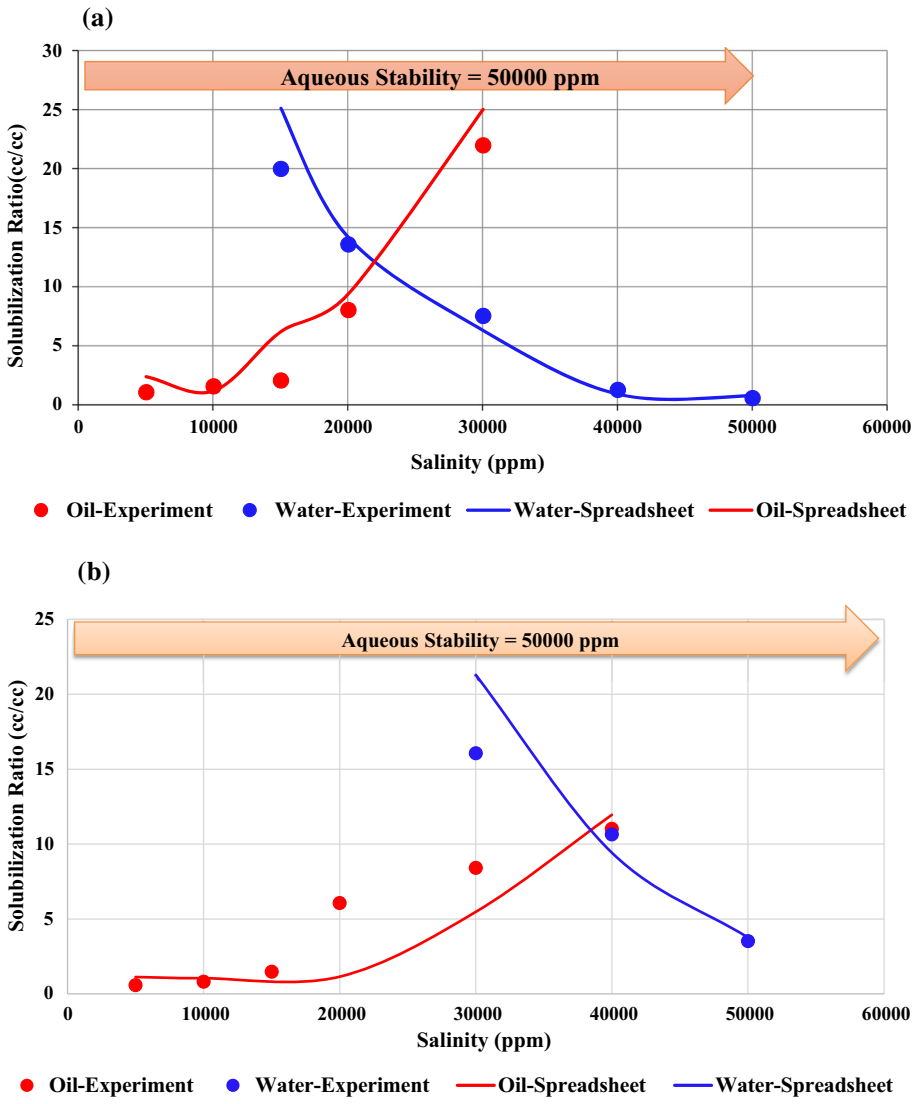

Fig. 6 Measured solubilization curves and fitted models for DSNS solutions, **a** DSNS solution with silica nanoparticles of 7 nm, **b** DSNS solution with silica nanoparticles of 25 nm

Table 5 Tuned parameters of phase behavior experiments based on the spreadsheet model

Sample	HBNC70	HBNC71	HBNC72	CSEL7	CSEU7
DSNS (7 nm)	0.025	0.043	0.055	0.2138	0.65
DSNS (25 nm)	0.045	0.0430	0.055	0.4538	0.96

lization process. Furthermore, the hydrophilic nanoparticles make the bulk solution unfavorable for hydrophobic surfactant tails and increase their affinity to form micelles. Therefore, micelle aggregates form at lower concentrations, and the CMC reduced [36]. Overall, by analyzing the solubilization curves and based on the results of conductivity measurements, the addition of silica nanoparticles to the SDS solution can improve the solubilization ability of the SDS solution dramatically.

3.4 Stability Investigation of the Optimum Solutions

Regarding the results of solubilization curves, the optimum solutions are the DSNS solution of the silica nanoparticle size of 7 nm with optimum salinity of 22,000 ppm and the DSNS solution of the silica nanoparticle size of 25 nm with optimum salinity of 38,000 ppm. In this part, the stability of these solutions is examined. The zeta potential measurements revealed that the first solution has the zeta potential of equal to -28 mV $\pm$ 0.05% and the second solution has the zeta potential of equal to -27 mV $\pm$ 0.05%. These information declared that both solutions are stable for a relatively long time. Moreover, the results of UV–visible measurements are given in Table 7 for both solutions. Based on the results, the DSNS solution with the particle size of 7 nm is relatively more stable than the second solution. This difference between the absorbance of the solutions may be related to

Table 6 Conductivity of different chemical solutions versus surfactant concentration

Conductivity (μs/cm)	Surfactant concentration (ppm)	Fitted correlation
SDS solution (CMC = 2450 ppm)		
276.562	1000	$Y = 0.2228X + 53.762$
343.402	1300	
499.36	2000	
572.91	2200	$Y = 0.1216X + 305.39$
730.99	3500	
791.79	4000	
DSNS solution (particle size of 7 nm) (CMC = 2100 ppm)		
268.457	1000	$Y = 0.2186X + 49.857$
334.037	1300	
487.057	2000	
524.60	2200	$Y = 0.1418X + 212.64$
708.94	3500	
779.84	4000	
DSNS solution (particle size of 25 nm) (CMC = 1850 ppm)		
276	1000	$Y = 0.22X + 56$
342	1300	
496	2000	
512.81	2200	$Y = 0.1464X + 190.73$
703.13	3500	
776.33	4000	

Table 7 UV–visible absorbance of DSNS solutions in different times at 390 nm wavelength at 25 °C

Absorbance	Time (h)
DSNS solution (7 nm)	
0.2685	1
0.2685	6
0.2685	48
0.29	192
DSNS solution (25 nm)	
0.42	1
0.42	6
0.425	48
0.45	192

the higher salinity of DSNS solution with silica nanoparticle size of 25 nm. Based on the DLVO theory, electrostatic forces are strongly dependent on electrolyte concentration in dispersion. As the electrolyte concentration increases, the thickness of the diffuse electrical layer decreases and particles tend to aggregate. This decreases the repulsive forces between particles. Because the repulsive forces prevent the aggregation of particles, large electrolyte concentration allows the attractive van der Waals forces to dominate, and particles tend to aggregate [55].

3.5 Oil Displacement Processes

3.5.1 Experimental Results

Figure 7 shows the experimental results for the oil recovery factor as a function of injected pore volumes (PV) during water flood. The results from laboratory show that cumulative oil recovery is about 39% of IOIP at breakthrough time (BT) of the 0.43 PV. In addition, the ultimate oil recovery is 43% at 1 PV. Figure 8 displays the closed-up views of the porous medium showing the distribution of oil saturation at different parts of the micromodel during water flood. In addition, Fig. 9 depicts the distribution of oil saturation at the end of water flood. These results show that high amount of oil remained through porous media even after 1 PV of water flood. The pictures show that the high amount of oil was either bypassed or adhered to the surface mainly due to high capillarity and high IFT between oil and water leading to the low sweep efficiency for both central and marginal parts of the model. In addition, the existence of the thick oil layer on the porous medium walls and incomplete swept zones proved that the injection of water has a poor performance in reducing the oil saturation for both pore and pore throats.

The next flooding process was the injection of best chemical formulation in terms of IFT reduction which was DSNS solution with the particle size of 7 nm (at optimal salinity of 22,000 ppm). The experimental results are shown in Fig. 7. The results from experimental model indicate that cumulative oil recovery at BT is about 50% of IOIP and finally the injectant can recover the 57% of IOIP at 1 PV. More importantly, the ultimate oil recovery during DSNS flood is about 10% of IOIP greater than that of water flood. Figure 10 shows the closed-up views of the porous medium after 60 min of DSNS flood. In addition, Fig. 11 also shows the distribution of oil saturation at the end of DSNS flood. The pictures clearly show that the injection of DSNS solution into the porous medium dramatically reduced the thickness of the adhered oil to the surface. In fact, based on the results of conductivity measurements and analyzed solubilization curves, the ability of DSNS solution in reducing IFT and oil emulsification can improve the oil mobilization process. As the pictures show, the injection of DSNS solution can reduce the amount of residual oil at in both pores and pore throats which make a favorable sweep efficiency after DSNS flood.

Finally, to conduct a comparison between the performance of DSNS solution with the particle size of 7 nm and SDS solution, 1 PV of SDS solution without silica nanoparticles was injected into the micromodel. The injection scheme of SDS flood such as the salinity of injected solution, SDS concentration, and injection rate is the same as DSNS flood. The results of this comparison are depicted in Fig. 12. As the results show, DSNS flood can improve oil recovery 4% of IOIP greater than SDS flood. In addition, the amount of oil recov-

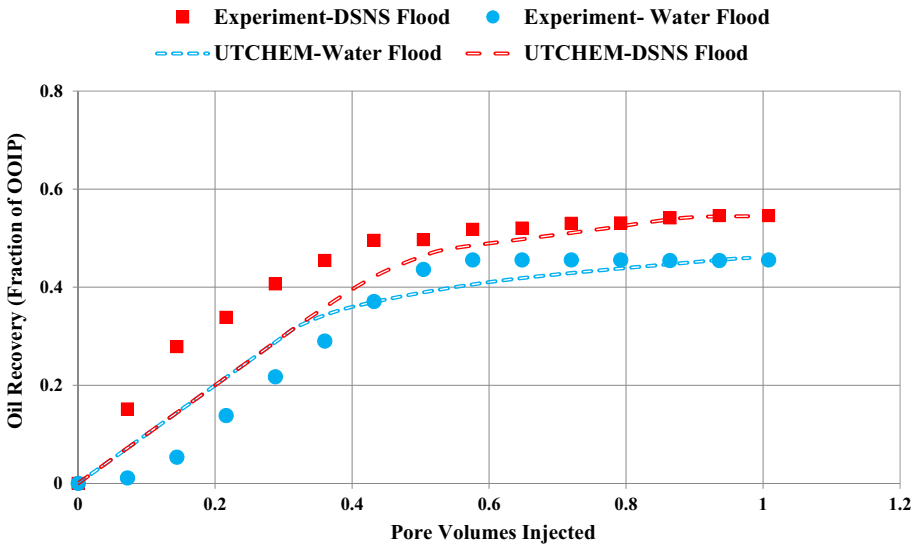

Fig. 7 Oil recovery match for water flood and DSNS flood

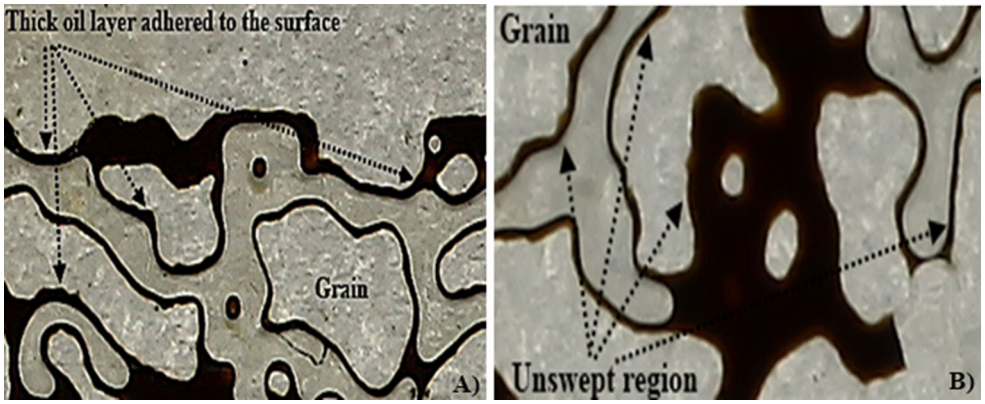

Fig. 8 Closed-up views of the porous medium after 60 min of water flood, **a** marginal part of the model, **b** central part of the model

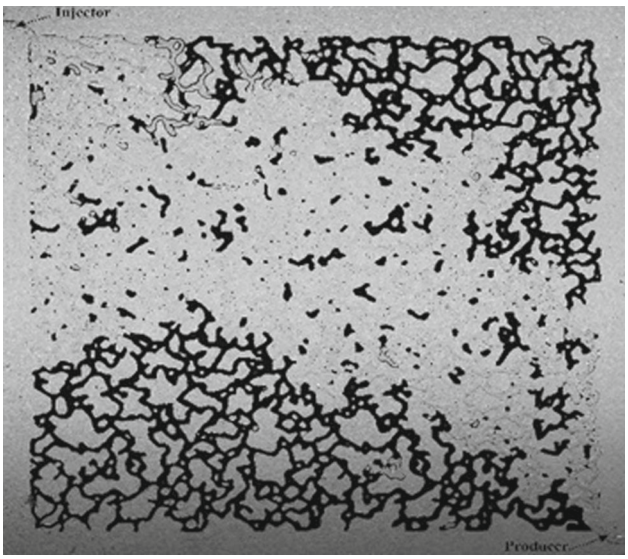

Fig. 9 Distribution of oil saturation at the end of water flood

ery at BT is relatively lower for conventional surfactant flood compared with DSNS flood. Based on the phase behavior tests, the assembly of silica nanoparticles and SDS improves the performance of the anionic surfactant in reducing IFT according to the Huh [12] equation. Moreover, stability of the surfactant solution was dramatically enhanced by the use of hydrophilic silica nanoparticles in high salinity conditions. As a result, the ability of DSNS solution for oil emulsification and IFT reduction are the main responsible factors for the improved oil recovery during DSNS flood.

To further clarify the results, Fig. 13 shows the comparison of the amount of residual oil distribution after conventional surfactant flood and DSNS flood. As the pictures show, the DSNS solution can spread over the marginal parts of the model and decrease the amount of oil saturation by reducing IFT and emulsifying the oil which is in complete agreement with the results of phase behavior tests. But the SDS solution can only swept the central parts of the model, thus having a poor sweep efficiency at the marginal parts.

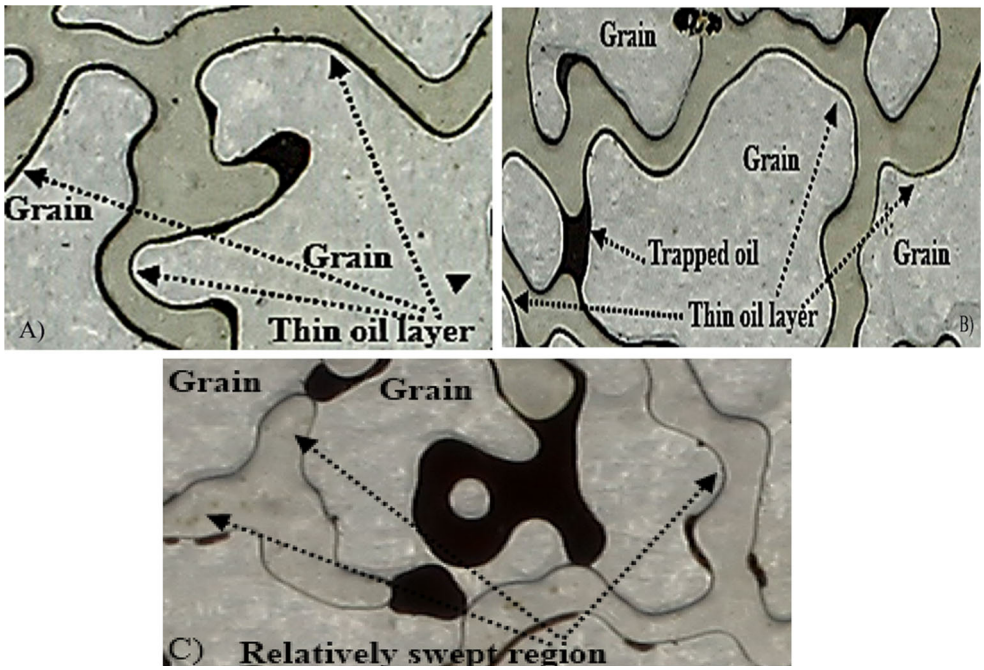

Fig. 10 Closed-up views of the porous medium after 60 min of DSNS flood, **a** thin oil layer adhered to the pore walls, **b** relatively low amount of residual oil at pore throats, **c** relatively high sweep efficiency of the porous medium

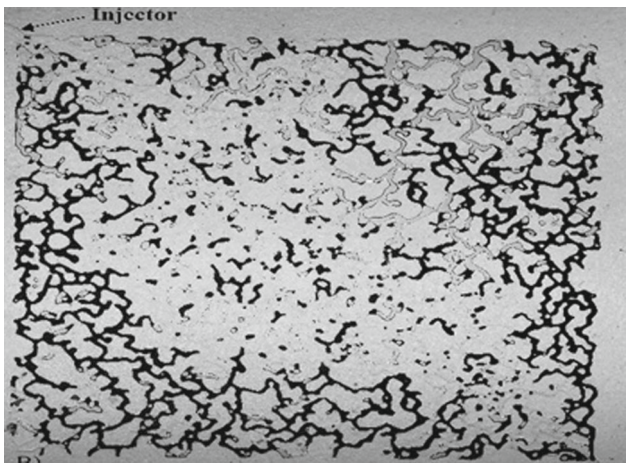

Fig. 11 Distribution of oil saturations at the end of DSNS flood

3.5.2 Simulation Results

Based on the simulation results for water flood (Fig. 7), the numerical model simulates the cumulative oil recovery slightly overestimating especially before BT, while the simulator predicts the experimental results accurately after BT. Generally, the agreement between simulation results compared with the experimental data is relatively good. Furthermore, the numerical model for DSNS flood (Fig. 7) simulates the cumulative oil recovery slightly underestimating especially before BT, while the numerical model predicts the experimental results precisely after BT. Generally, the agreement between simulation results compared with the experimental data is good.

4 Conclusion and Recommendations

The main findings of this work and some recommendations for further study can be summarized as follows:

1. A series of phase behavior experiments to study the impact of silica nanoparticles on the ability of SDS surfactant to reduce IFT were performed. The results showed that the addition of silica nanoparticles to the SDS solution can improve the emulsification ability of SDS surfactant and create the desirable IFT to mobilize trapped oil.
2. By the use of Huh [12] equation and comparison of the phase behavior results for DSNS solutions with different particle sizes, it can be concluded that silica nanoparticles smaller in size are more effective in reducing IFT. Moreover, the results of conductivity measurements proved that the addition of silica nanoparticles can reduce CMC of surfactant and improve the emulsification ability of the surface active agents.
3. The stability of optimum solutions was also examined by the use of zeta potential measurements and spectrophotometer experiments which indicated a relatively stable condition for the optimum solutions.

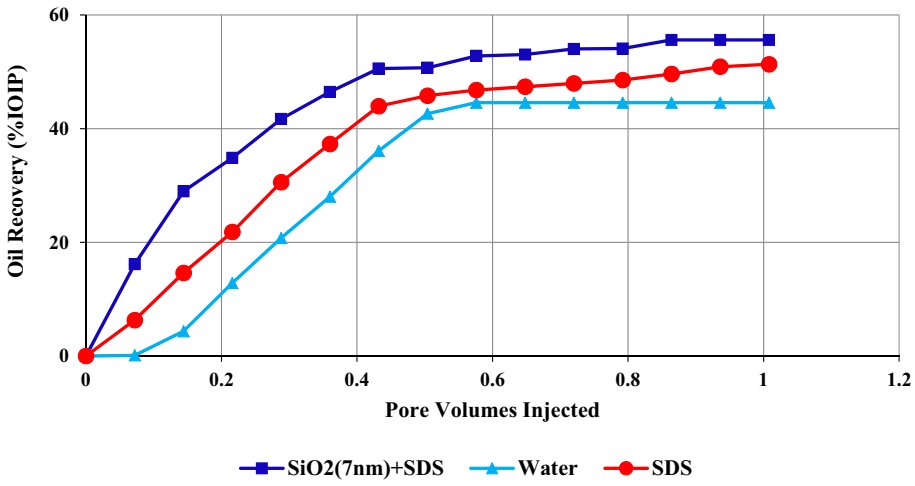

Fig. 12 Comparison of oil recovery for different injection schemes

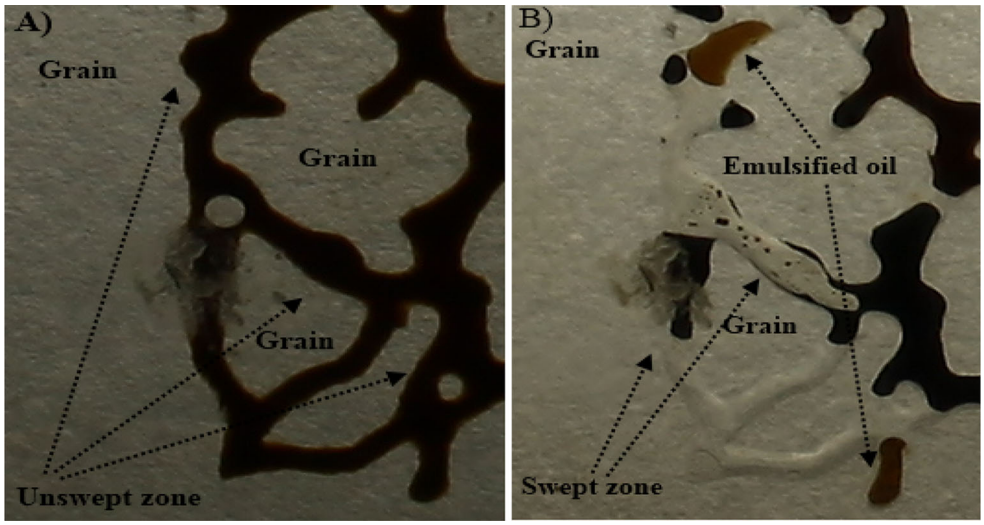

Fig. 13 Distribution of oil saturations at the marginal parts of the porous medium, **a** SDS flood, **b** DSNS flood

4. According to the properties of prepared solutions, the required input parameters for simulation of DSNS flood were successfully obtained by tuning the surfactant module of UTCHEM simulator. To the extent of our knowledge, this is the first time that the properties of DSNS solution are matched with chemical compositional simulator surfactant models to simulate DSNS flood.
5. Based on the oil recovery experiment conducted using a five-spot glass micromodel, 2D simulation model was constructed and history match of oil recovery data between simulation model and experimental results was carried out. The simulation results show that DSNS flood improves oil recovery up to 4% of IOIP greater than SDS flood. The improvement in the emulsification and IFT reduction abilities of the SDS by the use of silica nanoparticles are the main responsible mechanisms, during DSNS flood, for the higher ultimate oil recovery compared with the conventional surfactant flood.
6. In this paper, the effects of only two types of silica nanoparticles with different particle sizes were investigated. To have more reliable results, the same experimental procedure should be carried out to study the effect of silica nanoparticles with different particle sizes for different crude oil. Moreover, the interaction of the DSNS solution and the reservoir rock surface should be studied in future studies.

Acknowledgements The work was financially sponsored by Eqbal Lahoori Institute of Higher Education, in Mashhad (Iran). We would like to thank Nanosany Corporation for providing the authors with some laboratory materials. The authors thank Research Institute of Food Science and Technology (RIFST), in Mashhad, and Petro Ahoura Company, in Tehran, for the provision laboratory facilities. We would like to thank ESSS for providing the post-processor software needed to complete this work.

References

1. Sharma, H.; Panthi, K.; Mohanty, K.K.: Surfactant-less alkali-cosolvent-polymer floods for an acidic crude oil. Fuel **215**, 484–491 (2018). https://doi.org/10.1016/j.fuel.2017.11.079
2. Sheng, J.: Modern Chemical Enhanced Oil Recovery: Theory and Practice. Gulf Professional Publishing, Elsevier, Burlington (2011)
3. Dashti, G.: A Study of Microemulsion Viscosity with Consideration of Polymer and Co-solvents Additives. M.S. Thesis, The University of Texas at Austin, Austin, Texas (May 2014)
4. Karambeigi, M.S.; Nasiri, M.; Haghighi Asl, A.; Emadi, M.A.: Enhanced oil recovery in high temperature carbonates using microemulsions formulated with a new hydrophobic component. J. Ind. Eng. Chem. **39**, 136–148 (2016). https://doi.org/10.1016/j.jiec.2016.05.020
5. Jin, L.; Budhathoki, M.; Jamili, A.; Li, Zh.; Luo, H.; Delshad, M.; Shiau, B.; Harwell, J.H.: Predicting microemulsion phase behavior for surfactant flooding. In: Paper SPE 179701 (2016). https://doi.org/10.2118/179701-MS
6. Winsor, P.A.: Solvent Properties of Amphiphilic Compounds. Butterworth Scientific Publications, London (1974)
7. Yassin, M.R.; Ayatollahi, S.; Rostami, B.; Hasani, K.: Microemulsion phase behavior of a cationic surfactant at intermediate interfacial tension in sandstone and carbonate rocks. J. Energy Resour. Technol. **137**, 012905–012917 (2015)
8. Healy, R.N.; Reed, R.L.: Immiscible microemulsion flooding. SPE J. **17**, 129–139 (1977). https://doi.org/10.2118/5817-PA
9. Nelson, R.C.; Pope, G.A.: Phase relationship in chemical flooding. SPE J. **18**, 325–338 (1978). https://doi.org/10.2118/6773-PA
10. Lu, J.; Goudarzi, A.; Chen, P.; Kim, D.H.; Delshad, M.; Mohanty, K.K.; Sepehrnoori, K.; Weerasooriya, U.P.; Pope, G.A.: Enhanced oil recovery from high-temperature, high-salinity naturally fractured carbonates reservoirs by surfactant flood. J. Pet. Sci. Eng. **124**, 122–131 (2014). https://doi.org/10.1016/j.petrol.2014.10.016
11. Kamal, M.S.; Hussein, I.A.; Sultan, A.S.: Review on surfactant flooding: phase behavior, retention, IFT, and field applications. Energy Fuels **31**, 7701–7720 (2017)
12. Huh, C.: Interfacial tensions and solubilizing ability of a microemulsion phase that coexist with oil and brine. J. Colloid Interface Sci. **71**, 408–426 (1979). https://doi.org/10.1016/0021-9797(79)90249-2
13. Nelson, R.C.: The effect of live crude on phase behavior and oil-recovery efficiency of surfactant flooding. SPE J. **23**, 501–510 (1983). https://doi.org/10.2118/10677-PA
14. Escontrla, I.R.; Puetro, M.C.; Miller, C.A.; Soto, A.: Ionic liquids for low-tension oil recovery processes: phase behavior tests. J. Colloid Interface Sci. **504**, 404–416 (2017). https://doi.org/10.1016/j.jcis.2017.05.102
15. Healy, R.N.; Reed, R.L.; Carpenter Jr., C.W.: A laboratory study of microemulsion flooding. SPE J. **15**, 87–103 (1975). https://doi.org/10.2118/4752-PA
16. Hirasaki, G.J.; Van Domselaar, H.R.; Nelson, R.C.: Evaluation of the salinity gradient concept in surfactant flooding. SPE J. **23**, 486–500 (1983). https://doi.org/10.2118/8825-PA
17. Levitt, D.B.; Jackson, A.C.; Heinson, C.; Britton, L.N.; Malik, T.; Dwarakanath, V.; Pope, G.A.: Identification and evaluation of high-performance EOR surfactants. SPE Reserv. Eval. Eng. **12**, 243–253 (2006). https://doi.org/10.2118/100089-PA
18. Dwarakanath, V.; Chaturvedi, T.; Jackson, A.C.; Malik, T.; Siregar, A.; Zhao, P.: Using co-solvents to provide gradients and improve oil recovery during chemical flooding in a light oil reservoir. In: Paper SPE 113965 (2008). https://doi.org/10.2118/113965-MS
19. Awang, M.B.; Dzulkarnani, I.B.; Wahyudeen, B.Z.M.: Enhancement of IFT reduction in surfactant flooding by branched alcohols. In: Paper IPTC 15140 (2011). https://doi.org/10.2523/IPTC-15140-MS
20. Khalilinezhad, S.S.; Cheraghian, G.; Roayaei, E.; Tabatabaee, H.; Karambeigi, M.S.: Improving heavy oil recovery in the polymer flooding process by utilizing hydrophilic silica nanoparticles. Energy Sour. Part A Recov. Util. Environ. Eff. (2017). https://doi.org/10.1080/15567036.2017.1302521 (in press)
21. Khalilinezhad, S.S.; Cheraghian, G.; Karambeigi, M.S.; Tabatabaee, H.; Roayaei, E.: Characterizing the role of clay and silica nanoparticles in enhanced heavy oil recovery during polymer flooding. Arab. J. Sci. Eng. **41**, 2731–2750 (2016). https://doi.org/10.1007/s13369-016-2183-6
22. Zargartalebi, M.; Kharrat, R.; Barati, N.: Enhancement of surfactant flooding performance by the use of silica nanoparticles. Fuel **143**, 21–27 (2015). https://doi.org/10.1016/j.fuel.2014.11.040
23. Zargartalebi, M.; Barati, N.; Kharrat, R.: Influences of hydrophilic and hydrophobic silica nanoparticles on anionic surfactant properties: interfacial and adsorption behaviors. J. Pet. Sci. Eng. **119**, 36–43 (2014). https://doi.org/10.1016/j.petrol.2014.04.010
24. Vatanparast, H.; Javadi, A.; Bahramian, A.: Silica nanoparticles cationic surfactants interaction in water–oil system. Colloids Surf. A Physicochem. Eng. Asp. **521**, 221–230 (2017). https://doi.org/10.1016/j.colsurfa.2016.10.004
25. Biswal, N.R.; Rangera, N.; Singh, J.K.: Effect of different surfactants on the interfacial behavior of the *n*-Hexane-Water system in the presence of silica nanoparticles. J. Phys. Chem. B **120**, 7265–7274 (2016)
26. Esmaeilizadeh, P.; Hosseinipour, N.; Bahramian, A.; Fakhroueian, Z.; Arya, Sh: Effect of ZrO_2 nanoparticles on the interfacial behavior of surfactants at air–water and *n*-Heptane-Water interfaces. Fluid Phase Equilib. **361**, 289–295 (2014). https://doi.org/10.1016/j.fluid.2013.11.014
27. Ahmadi, M.-A.; Ahmed, Z.; Phung, L.T.K.; Kashiwao, T.; Bahadori, A.: Evaluation of the ability of the hydrophobic nanoparticles of SiO_2 in the EOR process through carbonate rock samples. Pet. Sci. Technol. **34**, 1048–1054 (2016). https://doi.org/10.1080/10916466.2016.1148052
28. AlamiNia, H.; Khalilinezhad, S.S.: Application of Hydrophilic Silica Nanoparticles in Chemical Enhanced Oil Recovery Processes. Energy Sources Part A Recovery Util. Environ. Eff. (2017). https://doi.org/10.1080/15567036.2017.1299257 (in press)
29. Ahmadi, M.-A.; Ahmed, Z.; Phung, L.T.K.; Kashiwao, T.; Bahadori, A.: Experimental investigation of the effect of nanoparticles on micellization behavior of a surfactant: application to EOR. Pet. Sci. Technol. **34**, 1055–1061 (2016). https://doi.org/10.1080/10916466.2016.1148051
30. Cheraghian, G.; Khalilinezhad, S.S.: Improvement of heavy oil recovery and role of nanoparticles of clay in the surfactant flooding process. Pet. Sci. Technol. **34**, 1397–1405 (2016). https://doi.org/10.1080/10916466.2016.1198805
31. Ahmadi, M.A.: Use of nanoparticles to improve the performance of sodium dodecyl sulfate flooding in a sandstone reservoir. Eur. Phys. J. Plus **131**, 435 (2016). https://doi.org/10.1140/epjp/i2016-16435-5
32. Cheraghian, G.; Kiani, S.; Nassar, N.N.; Alexander, S.; Barron, A.: Silica nanoparticles enhancement in the efficiency of surfactant flooding of heavy oil in a glass micromodel. Ind. Eng. Chem. Res. **56**, 8528–8534 (2017)
33. Khorsand, H.; Kiayee, N.; Masoomparast, A.H.: Optimization of amorphous silica nanoparticles synthesis from rice straw ash using design of experiment technique. Part. Sci. Technol. **31**, 366–371 (2013). https://doi.org/10.1080/02726351.2012.755587
34. Jafari, V.; Allahverdi, A.; Vafaei, M.: Ultrasound-assisted synthesis of colloidal nanosilica from silica fume: effect of sonication time on the properties of product. Adv. Powder Technol. **25**, 1571–1577 (2014). https://doi.org/10.1016/j.apt.2014.05.011

35. Metin, C.O.; Lake, L.W.; Miranda, C.R.; Nguyen, Q.P.: Stability of aqueous silica nanoparticles dispersions. J. Nanopart. Res. **13**, 839–850 (2011)
36. Ahmadi, M.-A.; Sheng, J.: Performance improvement of ionic surfactant flooding in carbonate rock samples by use of nanoparticles. Pet. Sci. **13**, 725–736 (2016). https://doi.org/10.1007/s12182-016-0109-2
37. https://www.kruss.de/fileadmin/user_upload/website/brochures/kruss-bro-k100-en.pdf
38. Ghahremani, H.; Mobaraki, S.; Khalilinezhad, S.S.; Jarrahian, K.: An experimental study of the performance of low-molecular weight polymer for enhanced heavy oil recovery in a heterogeneous media. Geosyst. Eng. **21**, 95–102 (2017). https://doi.org/10.1080/12269328.2017.1385424
39. Mohammadi, S.; Maghzi, A.; Ghazanfari, M.H.; Masihi, M.; Mohebbi, A.; Kharrat, R.: On the control of glass micromodel characteristics developed by laser technology. Energy Resources Part A Recovery Utili. Environ. Eff. **35**, 193–201 (2013). https://doi.org/10.1080/15567036.2010.516325
40. Khalilinezhad, S.S.; Cherghian, G.: Mechanisms behind injecting the combination of nano-clay particles and polymer solution for enhanced oil recovery. Appl. Nanosci. **6**, 923–931 (2016). https://doi.org/10.1007/s13204-015-0500-0
41. Levitt, D.: Experimental Evaluation of High Performance EOR Surfactants for a Dolomite Oil Reservoir. M.S. Thesis, The University of Texas at Austin, Austin, Texas (2006)
42. Flaaten, A.; Nguyen, Q.P.; Pope, G.A.; Zhang, J.: A systematic laboratory approach to low-cost, high-performance chemical flooding. SPE Reserv. Eval. Eng. **12**, 713–723 (2009). https://doi.org/10.2118/113469-PA
43. Emami Meybodi, H.; Kharrat, R.; Wang, X.: Study of microscopic and macroscopic displacement behaviors of polymer solution in water-wet and oil-wet media. Transp. Porous Media **89**, 97–120 (2011). https://doi.org/10.1007/s11242-011-9754-5
44. UTCHEM-9.0.: A Three-Dimensional Chemical Flood Simulator, Volumes 1 and 2, Reservoir Engineering Research Program, Center for Petroleum and Geosystems Engineering. The University of Texas, Austin (2000)
45. Goudarzi, A.; Delshad, M.; Sepehrnoori, K.: A chemical EOR benchmark study of different reservoir simulators. Comput. Geosci. **94**, 96–109 (2016). https://doi.org/10.1016/j.cageo.2016.06.013
46. Anderson, G.A.: Simulation of Chemical Flood Enhanced Oil Recovery Processes Including the Effects of Reservoir Wettability. M.S. Thesis, The University of Texas at Austin, Austin, Texas (2006)
47. Green, D.W.; Willhite, G.P.: Enhanced oil recovery. In: Memorial Found, Society of Petroleum Engineers. The University of Kansas, Lawrence, Kansas (1998)
48. Healy, R.N.; Reed, R.L.: Physicochemical aspects of microemulsion flooding. SPE J. **14**, 491–501 (1974). https://doi.org/10.2118/4583-PA
49. Hand, D.B.: Dineric distribution: I. The distribution of a consolute liquid between immiscible liquids. J. Phys. Chem. **34**, 1961–2000 (1939)
50. Veedu, F.K.: Scale-Up Methodology for Chemical Flooding. M.S. Thesis, The University of Texas at Austin, Austin, Texas (2010)
51. Mohammadi, H.; Delshad, M.; Pope, G.A.: Mechanistic modeling of alkaline/surfactant/polymer floods. SPE Reserv. Eval. Eng. **12**, 518–527 (2009). https://doi.org/10.2118/110212-PA
52. AlSofi, A.M.; Liu, J.S.; Han, M.; Aramco, S.: Numerical simulation of surfactant-polymer coreflooding experiments for carbonates. J. Pet. Sci. Eng. **111**, 184–196 (2013). https://doi.org/10.1016/j.petrol.2013.09.009
53. Ravera, F.; Santini, E.; Loglio, G.; Ferrari, M.; Liggieri, L.: Effect of nanoparticles on the properties of liquid/liquid and liquid/air surface layers. J. Phys. Chem. B **110**, 19543–19551 (2006)
54. Ahualli, S.; Iglesias, G.R.; Wachter, W.; Dulle, M.; Minami, D.; Glaatter, O.: Adsorption of anionic and cationic surfactants on anionic colloids: supercharging and destabilization. Langmuir **27**, 9182–9192 (2011)
55. Azadgoleh, J.E.; Kharrat, R.; Barati, N.; Sobhani, A.: Stability of silica nanoparticle dispersion in brine solution: an experimental study. Iran. J. Oil Gas Sci. Technol. **3**, 26–40. (2014) http://ijogst.put.ac.ir/article_7485.html